Reinforcing and Toughening of Polypropylene With Self-Assembled Low Molar Mass Additives

O. Sinan Yordem,[1] Adriane G. Simanke,[2] Alan J. Lesser[1]
[1] *Department of Polymer Science and Engineering, University of Massachusetts, Amherst, Massachusetts 01003-9263*

[2] *Innovation and Technology Center—Braskem SA, III Polo Petroquimico, 95853-000, Triunfo, Brazil*

This study presents a new approach to reinforce and toughen thermoplastic polymers by using a low molecular weight additive; calcium stearate ($CaSt_2$). The method involves melt blending isotactic polypropylene (iPP) and $CaSt_2$ at a process temperature where the $CaSt_2$ reduces the process viscosity through its characteristic morphology. Once the mixture cools, $CaSt_2$ coalesces and solidifies to develop reinforcing domains. Differential scanning calorimeter experiments demonstrate a significant reduction in the percent crystallinity of iPP with the addition of $CaSt_2$. The changes in yield strength and modulus suggest a synergistic effect between the $CaSt_2$ domains and iPP. Addition of 10% $CaSt_2$ increases the fracture energy by almost four-fold with a simultaneous increase in the elastic modulus. The melt flow rate of the composite is dramatically increased with $CaSt_2$ incorporation. Reduction in coefficient of thermal expansion was also observed. Simultaneous positive effects of $CaSt_2$ filler is attributed to its rich mesomorphic structure and its interaction with the iPP matrix. POLYM. ENG. SCI., 51:550–558, 2011. © 2010 Society of Plastics Engineers

INTRODUCTION

Toughening of semicrystalline polymers continues to be an active area of research and development. The mechanisms by which polymer materials are toughened have been widely studied both experimentally and theoretically [1]. Although several methods have been adopted to toughen semicrystalline polymers, the most efficient and successful way has been to incorporate a dispersed rubbery phase within the semicrystalline matrix. It is well accepted that this method can increase the fracture energy several fold if the appropriate toughening mechanisms are activated. One of these mechanisms includes the cavitation of rubber particles prior to catastrophic failure of the material. In most commercial systems, it has been shown that this method of improving the impact toughness occurs in volume concentration ranges up to 20%. However, the introduction of the rubbery phase has a detrimental effect on the stiffness, yield strength, and processability of the material.

Another more-recent method to increase the fracture toughness involves incorporating discrete rigid particles that can debond or dewet at excessive stress levels. In 1999, Argon showed a successful way to toughen semicrystalline polymers through the incorporation rigid particle fillers [2]. The key to this approach involves first insuring that the particle-polymer interface is sufficiently weak to allow for particle to debond from the matrix at some excess stress level, followed by plastic deformation of the matrix. The primary benefit of rigid particle toughening over traditional soft particle toughening is that both modulus and toughness can be improved in the polymer. At low (service) stress levels, the interface between the rigid particles and polymer matrix remain intact allowing for load transfer to occur between the particles and matrix. This, in turn, leads to an increase in modulus as opposed to a decrease as seen in rubber modified systems. Once the stress levels increase to an excessive level, the particle-matrix interface fails (debonds) and provides a relief to dilatational stress much like cavitation of rubber particles do in soft-particle toughened systems. The relief of dilatational stress by debonding activates other energy absorbing mechanisms in the matrix similar to rubber modified systems after cavitation. Thus, many parallel arguments can be made with regard to particle size and concentration for both rubber toughened and rigid particle toughened systems. This is depicted in Fig. 1.

The graph in Fig. 1 demonstrates the effect that particle (soft or rigid) size and concentration have on the composite modulus and toughness. It should be noted that, for a fixed concentration, a decrease in particle size leads to a commensurate decrease in particle spacing thereby pro-

Correspondence to: Alan J. Lesser; e-mail: ajl@polysci.umass.edu
Contract grant sponsor: Braskem SA.
DOI 10.1002/pen.21860
Published online in Wiley Online Library (wileyonlinelibrary.com).

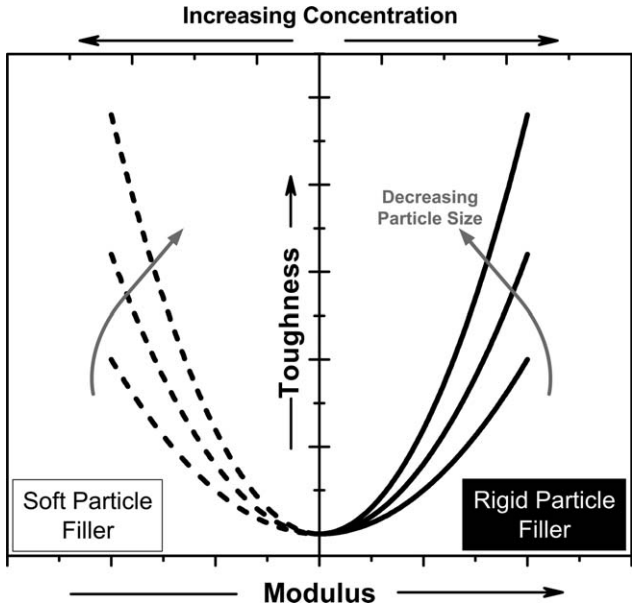

FIG. 1. Effect of particle concentration and size on the polymer modulus and toughness is depicted. Solid lines correspond to rigid particles; dashed lines represent soft particles.

viding more efficient particle-particle interaction and delocalization of failure during the fracture event.

However, one of the major drawbacks to these toughening strategies is that the melt viscosity of the systems increases tremendously, therefore reducing the processability of the polymer [3] and causing difficulty in developing the appropriate dispersion of filler for the case of rigid particles.

To address the process issue in rigid-particle reinforced systems, our group proposed to use low molecular weight crystallizable solvents for toughening and reinforcement [4, 5]. The strategy in this case is to have the crystallizable additive melt and become miscible at process temperatures thereby reducing the melt viscosity of the polymer. As the polymer cools, the additive undergoes thermally induced phase separation followed by crystallization to produce a dispersion of crystallites with the necessary morphology to provide toughening and modulus enhancement much like that reported by Argon. However, early attempts at this approach showed that the composites produced had a pronounced sensitivity to thermal history and both the crystal morphology of the polymer and additive can be affected. Also, many low molecular weight additives show a pronounced super-cooling response that detrimentally affects the response of the final composites [5].

This study is the second part in a series on investigating the utility of low molecular weight (LMW) compounds for reinforcing and toughening polymers. In this article, the strategy involves incorporating a LMW metal soap, calcium stearate ($CaSt_2$), in a polymer matrix at the processing temperature, and the fatty acid molecule evolves through coassembly to provide reinforcing domains similar in morphology to that required for rigid-particle toughening. We investigate the addition of $CaSt_2$ to simultaneously improve the fracture response of isotactic polypropylene and enhance the tensile modulus as well as processability. This approach is incorporated in a recent patent filing by the University of Massachusetts at Amherst [4].

Metal soaps, also known as fatty acid salts, are common additives in the plastics industry and used as lubricants, heat stabilizers, and antiscorching agents [6, 7]. A few studies utilizing metal soaps as rigid-particle reinforcing additives have been reported. The reinforcing properties of metal soaps as crystalline polar additives were only studied in highly associated ionic macromolecules. Lundberg and coworkers reported a marked improvement in the melt viscosity, tensile strength, elongation at break, and swelling of sulfonate containing ethylene-propylene-diolefin terpolymer (EPDM) ionomers with the addition of metal stearates such as zinc stearate [8–10]. Weiss reported similar studies on sulfonated-EPDM ionomer where the thermal, crystallization, and dissolution behaviors of zinc stearate in the ionomer were investigated [11–13]. Weiss also reported an enhanced shape memory effect in ionomers by the introduction of fatty acid salts [13]. Wakabayashi and Register utilized saturated and unsaturated fatty acid salts of magnesium and sodium to plasticize and reinforce ethylene/(meth)acrylic acid ionomers. They suggested that coassembly of the magnesium stearate and the ionomer brings synergistic effects towards increasing the modulus by three folds [14]. The reinforcing effect of metal soaps reported in these studies was bridged to the synergistic effect between the ionomers and fatty acid derivatives. Although enhanced mechanical properties were attained in ionomers, neither a detailed fracture mechanism of these composites, nor the use of metal soaps as a coassembled reinforcing and toughening additive in semicrystalline polymers was exemplified.

EXPERIMENTAL

Sample Preparation

Isotactic polypropylene, in pellet form, was supplied by Braskem, Brazil. The original neat polymer has a melt flow index of 3.5 g/10 min (2.16 kg at 230°C) and density of 0.905 g/cm^3. The calcium stearate filler was purchased from Alfa Aesar and used without further purification. All chemicals were dried under vacuum at 50°C overnight before use.

Compression molded specimens were prepared at UMass. First, the iPP pellets were cryo-grinded in a SPEX CertiPrep 6800 Freezer/Mill. One cycle consisted of 5 min of precooling and 3 min of cooling-grinding steps at a grinding rate of 13 impacts/second/side. After five cycles of cryo-grinding, fine polymer flakes were obtained. The iPP and $CaSt_2$ powder were dry-mixed in a

bag by shaking the bag vigorously. The mixture was then manually fed into a Brabender batch mixer at 200°C, which was purged with nitrogen gas before and during the mix. Blends of 10 and 20 weight% (wt%) of $CaSt_2$ were mixed for 3 min. Samples were finally quenched in water and vacuum dried overnight. Rectangular plaques of each composite batch were compression molded in a 40-ton PHI Manual Compression Press at 25tonnes and 230°C for 3 min.

Injection molded specimens were prepared at Braskem Laboratories. Isotactic-PP and $CaSt_2$ powder were dry mixed at 25 rpm for 5 min in a Mixaco mixer. The mixture was extruded in a Coperion ZSK 18 twin screw type extruder with a length/diameter ratio (L/D) of 18, operated at 250 rpm with a barrel mixing temperature profile of 200°C/200°C/205°C/205°C/205°C/210°C/215°C. The injection molded samples were produced in an Arbur 270U equipment, according to ASTM D4101. Different sample types were prepared in the injection molder: ASTM D-638 Type I for stress/strain analysis; ASTM D-256 for Izod impact test ($63.5 \times 10.16 \times 3.2$ mm^3 bars); ASTM D-790 for flexural modulus ($127 \times 13 \times 3$ mm^3 bars); and ASTM 648 for heat deflection temperature (HDT) measurements ($127 \times 13 \times 3$ mm^3 bars).

Rheology

Indirect measurement of viscosity was obtained by using Ceast Modular Flow Index (MFI) instrument, following ASTM D1238. Five grams of each batch with different $CaSt_2$ concentrations was packed inside the MFI instrument barrel. Samples were preheated to 230°C for 3 min. After the preheating, a specified weight was introduced onto the piston. Gravimetric weights of 2.16 kg, 5 kg, and 10 kg were used to screen the effect of pressure on material flow.

Thermal Properties

Differential scanning calorimeter (DSC) was utilized to monitor the change in crystallization and melting points, percent crystallinity, and the enthalpy of crystallization of the iPP matrix, before and after the incorporation of the $CaSt_2$ additive. Samples of approximately 5 mg were taken from the compression molded plaques and analyzed using a TA Instruments Q200 DSC. The instrument was calibrated by using sapphire disks and keeping the helium flow rate constant at 25 μl/min. Two heating and cooling cycles were employed between −50°C and +250°C with a constant ramp rate of 10°C/min. Crystallization and melting analyses were performed on the first cooling and the second heating ramps.

Additional thermal characterization was conducted at Braskem Laboratories. HDT measurements were carried out in a Ceast HDT*VICAT - AUTO equipment according to ASTM D648 at a heating rate of 2 ± 0.2°C/min. Coefficient of linear thermal expansion (CLTE) measurements were carried out in a TA Instruments 2950 TMA instrument according to ASTM D696. Samples with 3.1 mm diameter were machined from Izod specimen and the reported values represent the average of at least two measurements.

Mechanical Property Characterization at UMass

ASTM D638 Type V tensile test specimens were punched from compression molded plaques and were tested in an Instron 5800 universal testing machine (UTM) at room temperature. The crosshead displacement rate was 10 mm/min and the strain was calculated from the crosshead displacement. Elastic modulus, tensile strength, and elongation at break of both modified and unmodified samples were measured. Reported values were averaged over 10 measurements.

Single edge notched beam (SENB) rectangular bar specimens with dimensions of $42 \times 8.7 \times 3.5$ mm^3 were machined from 4 mm thick plaques. Specimens were tested in an Instron 5800 UTM with a crosshead displacement rate of 50 mm/min. Total fracture energies were calculated following the ASTM-E1280 standard.

Mechanical Property Characterization at Braskem Laboratories

Tensile properties were measured at room temperature using an Instron 4466 testing machine in accordance to the ASTM D638 using Type I specimen dimensions. A crosshead speed of 10 mm/min was employed and the average value of 10 specimens was taken for each sample.

The notched Izod impact strength was measured using a pendulum-type Ceast 6545 at 23°C with an impact speed of 3.46 m/s according to ASTM D-256. The reported values were averaged over 10 measurements. The standard specimen dimension is $63.5 \times 10.16 \times 3.2$ mm^3 (notched angle of $45 \pm 1°$ with a radius of curvature at the top of the notch of 0.25 ± 0.05 mm).

The flexural modulus was measured at room temperature using an Instron 4466 testing machine according to ASTM D790, at a crosshead speed of 13 mm/min.

Morphology

A Zeiss Evo50 Scanning Electron Microscopy (SEM) was used for the morphological analysis of cryo-fractured samples. Compression molded plaques were machined into 2×6 cm^2 rectangular specimens which were notched to a depth of 1 mm and cryo-fractured in a flexure setup. Fractured surfaces were sputter- coated with a thin layer of gold (~30 nm) prior to analysis.

Crystal structures of the composite samples were analyzed by using a simultaneous measurement of small-angle (SAXS) and wide-angle X-Ray scattering (WAXS) by a Rigaku S-Max3000 X-Ray instrument with a Cu-K_α radiation source.

 DOI 10.1002/pen

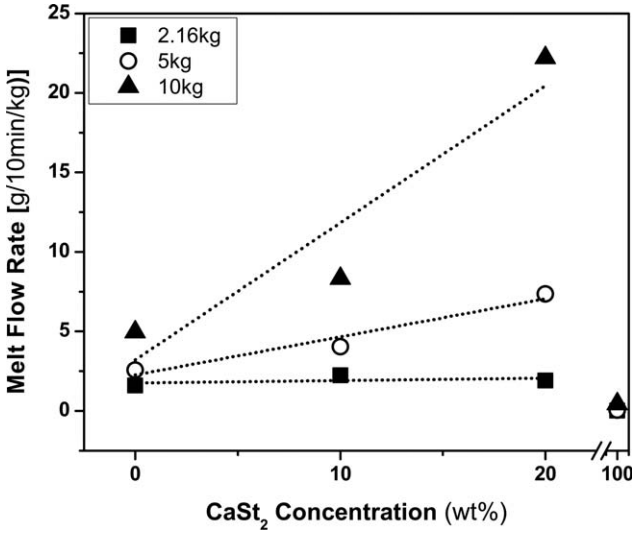

FIG. 2. Melt flow rate of composites at 230°C. Melt Flow Index values are normalized with respect to the gravimetric weights to provide the melt flow rate.

RESULTS AND DISCUSSION

Rheology

One of the significant drawbacks of rubber and $CaCO_3$ fillers in commercial systems is the tremendous increase in the process viscosity of the matrix [3]. However, $CaSt_2$ outperforms these modifiers by demonstrating a substantial improvement in the processability. Figure 2 shows the significant increase in the melt flow rate of iPP with the incorporation of $CaSt_2$. Effect of $CaSt_2$ is much more pronounced at heavier gravimetric weights. This suggests that at high shear rates, $CaSt_2$ eases the flow of iPP resin. Similar to our findings, Makowski and Lundberg, and Riley demonstrated increased melt flow in metal stearate filled EPDM ionomers and poly(vinyl chloride), respectively [8, 15].

Luzzati and Spegt demonstrated that stearates with divalent metals have a tendency to form bilayers like lipid molecules. They have shown a long range organization of the metal soaps which is strictly periodic in multi dimensions, yielding a mesomorphic structure. The reduced viscosity in the iPP-$CaSt_2$ blend is attributed to the cocontinuous bilayer morphology of $CaSt_2$ formed at elevated temperatures. Melt flow rate of neat (100%) calcium stearate given in Fig. 2 demonstrates that the $CaSt_2$ in its bulk is gel-like and extremely viscous. However, once the $CaSt^2$ is introduced into the iPP resin, the interaction between iPP chains and the short hydrocarbon tails of $CaSt^2$ in the cocontinuous phase results in an increased flow rate at higher shear rates and temperatures.

TABLE 1. Data collected from consecutive heating and cooling DSC scans of the composite specimens.

Specimen	T_c peak (°C)	T_m peak (°C)	ΔH_m (J/g)	Normalized% crystallinity[a]
Neat iPP	112.8	166.8	111.2	53.7
iPP-$CaSt_2$10	111.5	164.5	98.4	52.8
iPP-$CaSt_2$20	111.4	164.8	77.5	46.8

[a] Calculated from normalized ΔH_m values, using ΔH_m 207 J/g for 100% crystalline iPP [18].

Thermal Data

In general, metal soaps such as $CaSt_2$ do not exhibit any true melting behavior; rather, they soften at an elevated temperature. When they are heated to even higher temperatures, they exhibit further additional phase transitions where different liquid-crystalline-like orders are formed within the same sample [16, 17]. The formation of these mesomorphic $CaSt_2$ phases may alter the crystallization and melting behavior of iPP matrix. Relevant results from DSC experiments are given in Table 1.

Mixing $CaSt_2$ particles with polypropylene matrix does not result in any significant change (~1°C) in the crystallization temperatures of the iPP. However, there is a

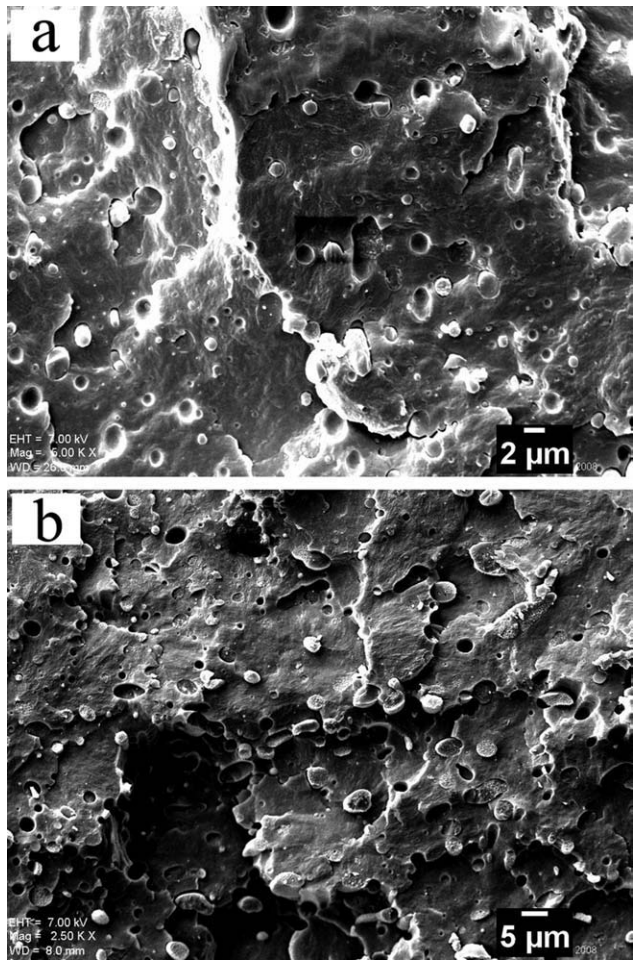

FIG. 3. Morphology of the $CaSt_2$ particles dispersed in the iPP matrix: middle sections of (a) the iPP-$CaSt_2$10 sample, and (b) the iPP-$Cast_2$20 sample.

TABLE 2. Calcium stearate particle size distribution.

Specimen	Filler volume fraction (%)	Average particle size[a] (μm)	Average particle circularity
iPP-$CaSt_2$10	9	1.08 ± 0.64	0.991 ± 0.029
iPP-$CaSt_2$20	18	2.01 ± 1.05	0.985 ± 0.032

[a] $CaSt_2$ particle size is averaged over 50 measurements obtained from the SEM images of cryo-fractured samples.

slight decrease (~3°C) in the melting peaks with the addition of $CaSt_2$. Overall, the effect of increasing $CaSt_2$ concentration does not appear to directly correlate with the observed changes in melting temperatures. Of note is that the normalized percent crystallinity values indicate significant reduction in the iPP crystallinity with increasing $CaSt_2$ concentration.

The full width at half maxima measured from the crystallization exotherms, which are not reported here, decreases with 10% $CaSt_2$ loading and increases with 20% $CaSt_2$ loading. This suggests that iPP spherulites have a narrower crystal size distribution with addition of 10wt% $CaSt_2$, and a broader size distribution with 20wt% of $CaSt_2$ filler. The complexity in the mesomorphic structures of $CaSt_2$ embedded within the iPP matrix makes this system difficult to interpret and is beyond the scope of this contribution.

Particle Size

The $CaSt_2$ particles as seen in Fig. 3 have a relatively uniform dispersion at low weight fractions. Filler agglomeration was minimal and the reinforcing domains are spherical in the bulk. It is important to note this spherical geometry of the LMW organo-metallic domains because organic crystals usually grow in faceted geometries, as previously shown by our group [4, 19, 20]. Regarding the interface between the particle and the matrix, and particle debonding from the matrix, the circular morphology and geometry of the fillers is significant under an applied load.

The average sizes of the particles for two different $CaSt_2$ weight fractions are given in Table 2. It is critical to note that the average $CaSt_2$ particle size is close to the optimum filler size of 0.7 μm in iPP as proposed by Argon and coworkers [21]. As $CaSt_2$ concentration is increased, the particle size and the size distribution of the particles increase. Besides, the particles tend to lose their circularity to some extent. This tendency will be discussed in the context of "Stratified Morphology". The complex morphologies of $CaSt_2$ particles are relevant for some of the mechanical responses and will be discussed in detail in the next section.

Tensile Properties

Tensile tests were conducted on both injection molded and compression molded specimens which were prepared in Braskem Chemical Co. Laboratories and at UMass laboratories, respectively. The collection of results is presented in Table 3.

Regardless of the processing method, the tensile strength and elongation at break values decreased with the addition of $CaSt_2$ filler. However, the changes do not correlate with the increasing concentration of $CaSt_2$. Rather, there exists a saturation limit for $CaSt_2$ concentration, above which the mechanical properties either do not change or decrease. The flexural modulus obtained from the injection molded bars exhibit an increase with the addition of $CaSt_2$. Although, the percent crystallinity of iPP matrix is decreased, introducing 10wt% of $CaSt_2$ increases the flexural modulus by 19%. The stiffening effect is accompanied with a possible coassembled morphology obtained with iPP chains and $CaSt_2$ molecules. A similar coassembled morphology was proposed by Lundberg and coworkers in the case of zinc stearate filled EPDM ionomers [8, 10]. Unlike our composite with iPP and $CaSt_2$, their material system comprises high ionic interactions. However, the short aliphatic tails in $CaSt_2$ can interact with iPP chains and form a coassembled, but weakly interacted, micelle-like micro domains. A detailed morphological study is required to explicitly understand the interaction between iPP matrix and $CaSt_2$ domains.

The compression molded samples have different absolute results but the overall trend is similar where sudden changes in the depression of yield stress and strain at break are observed. The initial decline in the yield stress with the addition of $CaSt_2$ is much sharper than the reduc-

TABLE 3. Tensile test results of injection molded and compression molded iPP-$CaSt_2$ composites.

	Injection-molded samples			Compression-molded samples.		
Sample	Young's modulus[a] (Gpa)	Yield strength (Mpa)	Elongation at break (mm)	Young's modulus (Gpa)	Yield strength (Mpa)	Elongation at break (mm)
Neat iPP	1.27 ± 0.01	36	696 ± 133	1.32 ± 0.6	37.8 ± 3.8	596.4 ± 37.0
iPP-$CaSt_2$5	1.51 ± 0.02	34 ± 1	196 ± 33	–	–	–
iPP-$CaSt_2$10	1.51 ± 0.01	33 ± 1	165 ± 17	1.31 ± 1.2	25.5 ± 1.1	341.0 ± 175.5
iPP-$CaSt_2$ 20[b]	1.49 ± 0.02	33	201 ± 15	1.2 ± 0.5	23.2 ± 1.3	93.0 ± 89.1

[a] Corresponds to the flexural modulus.

[b] $CaSt_2$ content of the injection molded iPP-$CaSt_2$20 samples are measured as 7wt%. This will be discussed in the context of Stratified Morphology.

TABLE 4. HDT and CLTE data of iPP-$CaSt_2$ composites.

Sample code	HDT (0.455 Mpa) (°C)	HDT (1.820 Mpa) (°C)	CLTE (μm/m°C)
Neat iPP	105 ± 2	58 ± 2	218
iPP-$CaSt_2$5	107 ± 1	60 ± 2	198
iPP-$CaSt_2$10	101 ± 1	59 ± 2	195
iPP-$CaSt_2$20	99 ± 3	58 ± 1	197

tions observed with increasing $CaSt_2$ concentration. Contrary to injection molded samples, the tensile modulus shows a slight reduction with increasing $CaSt_2$ concentration. Regarding the decreased percent crystallinity in iPP matrix, the discrete trend in the modulus demonstrates a slightly weaker stiffening effect. The reduction in elongation at break is not uncommon to observe in rigid particle filled systems. In our system, the elongation at break decreases tremendously as the size of the $CaSt_2$ particles become larger at higher concentration and act as flaws. Similar to injection molded specimens, a reduction in yield stress is also observed in the compression molded samples. A reduced yield strength is indicative of a debonding mechanism that one sees with typical rigid particle fillers [2, 21] that will be discussed next.

The size of the $CaSt_2$ particles given in Table 2 exhibits a distinct effect than the previously reported $CaCO_3$ fillers. Bartczak et al. showed that their material system gets slightly stiffer as $CaCO_3$ fillers get bigger in size; however, $CaSt_2$ particles present a stiffer response with smaller filler size. Furthermore, the mechanical response of the iPP-$CaSt_2$ composites is not controlled by the volume fraction of the modifier as discussed for $CaCO_3$ filled HDPE and iPP by Argon and coworkers [2, 21]. Additionally, a gradual depression in yield stress with an increase in particle size is not observed in $CaSt_2$. In fact, neither of the tensile properties demonstrates a gradual change with particle size or filler volume fraction. The results reported here indicate a potential existence of a synergistic effect between the $CaSt_2$ particles and the iPP matrix, in contrast to a $CaCO_3$ modified system where the effects are accredited to the volume fraction of the filler and the filler stiffness.

Coefficient of linear thermal expansion and heat deflection temperature results are shown in Table 4. The $CaSt_2$ filler is capable of decreasing the CLTE while the HDT of the iPP matrix is relatively unchanged. Presumably, the $CaSt_2$ domains have a lower CLTE than the iPP matrix resulting in a reduced composite CLTE. In addition, the reduction in CLTE is also associated with the decrease in the crystallinity of the iPP matrix.

Mechanism of Fracture

A reduction in yield stress indicates a dewetting mechanism occurring in the system and this effect was visually observed in the iPP-$CaSt_2$ composites. Upon the application of tensile force, samples immediately whitened throughout, suggesting the debonding of the particles from the matrix. Further investigation showed that the whitening was also due to the formation of crazes perpendicular to the loading direction during uniaxial tensile tests. Rapid dewetting of $CaSt_2$ domains, similar to the cavitation of rubber particles, relieves dilatational stress, changes the stress state in the matrix, and favors an enhanced toughening response.

Greater than a three-fold increase in total fracture energy (J_Q) and a 40% improvement in Izod values given in Fig. 4 indicate that the energy imparted to the material is dissipated. The fracture surface morphologies of the SENB specimens were analyzed under SEM to investigate possible fracture mechanisms. Neat iPP shows little or no plastic deformation as given in Fig. 5a. Whereas, the fracture surfaces of the $CaSt_2$ filled samples given in Fig. 5b and c show extensive plastic deformation of the iPP matrix, where debonding of the $CaSt_2$ particles is observed together with extensive fibrillation of the iPP matrix. The morphology of deformed domains and the effect of calcium stearate's complex morphology are still under investigation to better assess the fracture mechanism. The promising effect of $CaSt_2$ as reinforcing and toughening filler is important to note.

Crystallinity

WAXS experiments were conducted to monitor $CaSt_2$ crystal structure in the iPP matrix as well as changes in the crystallinity of iPP in the composites. The crystal information of iPP is reflected predominantly on the higher angle 2Θ peaks. The peak at 18.5° (Peak 4) in Fig. 6 is characteristic of the α-phase which suggests that the iPP matrix is predominantly in its α-form both in the neat polymer and in the iPP-$CaSt_2$ composites. As the $CaSt_2$ concentration is increased, the relative intensity of the iPP peaks at 21.1° (Peak 5) and 21.7° (Peak 6) change, and

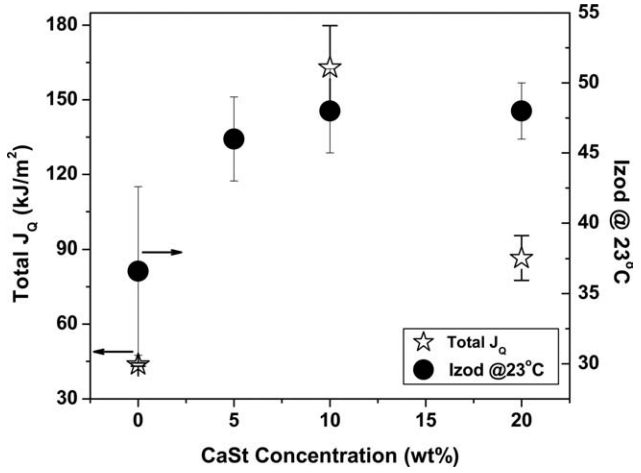

FIG. 4. Total fracture energy (J_Q) of compression molded SENB specimens, and Izod values of injection molded specimens.

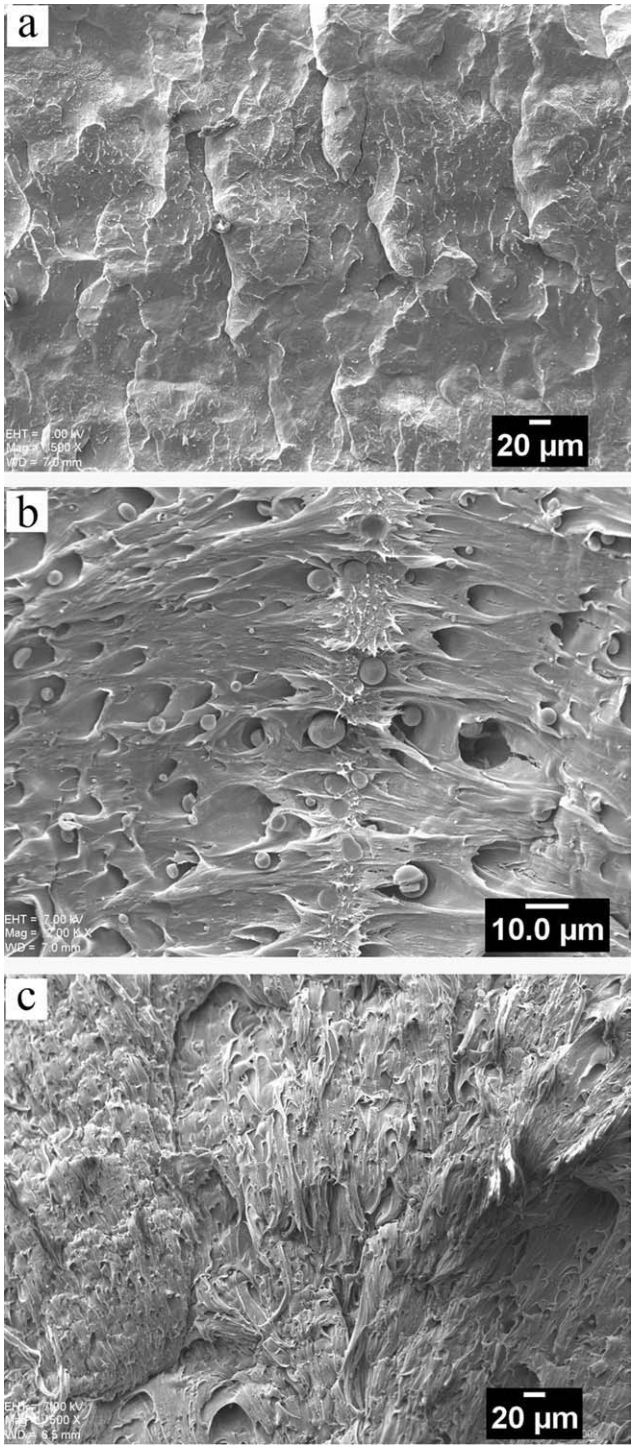

FIG. 5. Fracture surfaces of SENB specimens. (a) Neat iPP. (b) Dewetting of particles in iPP-$CaSt_2$10 sample. (c) Extensive fibrillation of the iPP-$CaSt_2$10 composite.

the peak at 16.8° (Peak 2) exhibits a significant decrease. An additional peak is also formed at 15.9° at the highest $CaSt_2$ loading, which is attributed to the (113) plane of a γ-form iPP crystal lattice. These results suggest that the crystal lattice structure of the iPP matrix is altered to some extent, but since the strong characteristic peak of the γ-phase at 20.27° is still absent, the change in crystallinity is not significant enough to completely transform the α-phase structure into a γ-phase. This is also corroborated by the slightly varied crystallization and melting temperatures obtained in DSC.

The short spacing peaks (around 10 2Θ) given in Fig. 6 do not reveal any information on the $CaSt_2$ crystallinity because the intensity of the iPP crystals in that range is higher. However, as the $CaSt_2$ concentration is increased, it is possible to see the trace of $CaSt_2$ molecules from the slight increase in the peak intensity at 9.05°. It is not possible to procure any additional information on the configuration of the $CaSt_2$ particles in the iPP matrix by looking at higher angle peaks due to the strong intensity of iPP.

STRATIFIED MORPHOLOGY

As the $CaSt_2$ filled iPP tensile bars were stretched, the outer layer of the specimens began to fail and "delaminate" during necking. The material continued to neck until other layers failed and this layered failure mechanism continued until the specimen fractured completely (Fig. 7a).

The layered failure mechanism is a consequence of the cocontinuous morphology of the $CaSt_2$ particles at the free surfaces, which was observed earlier in the literature and referred as the skin effect [22]. Figures 7b and 7c present the morphology of the $CaSt_2$ particles where the particle geometry deviates from spheres to ellipsoids with high anisotropy at the cocontinuous phase, in other words, at the skin of compression molded plaques (see arrows

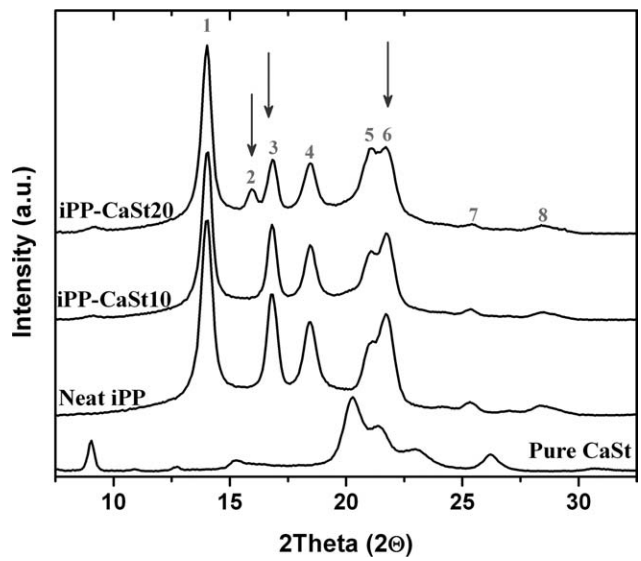

FIG. 6. 2D X-ray spectrums of iPP-$CaSt_2$ composites. Peaks numbered from 1 to 8 represent the peaks coming from the planes of iPP crystals: 1, (110) - α; 2, (113) – γ; 3, (040) - α or (008) – γ; 4, (130) – α; 5, (111) - α or (202) – γ; 6, (041) - α / (131) - α or (026) – γ; 7, (150) - α / (060) - α; 8, (200) - α planes.

DOI 10.1002/pen

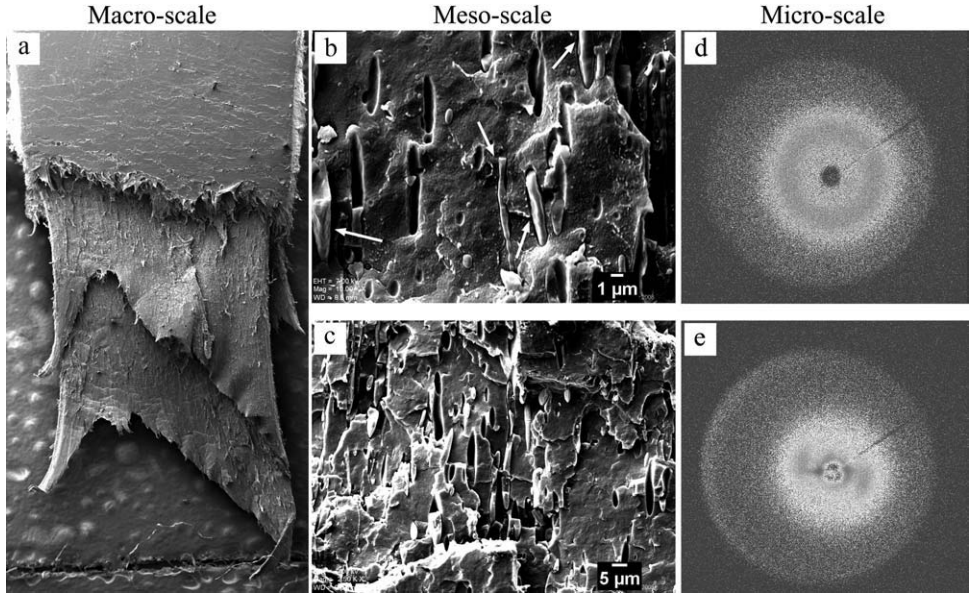

FIG. 7. Skin effect of $CaSt_2$ is illustrated. (a) Tensile bar specimen showing a layered fracture mechanism. Cocontinuous morphology of $CaSt_2$ particles from the fracture surfaces of the cryo-fractured (b) iPP-$CaSt_2$10, and (c) iPP-$CaSt_2$20 samples. SAXS images of (d) Neat iPP and (e) iPP-$CaSt_2$20 specimens show the orientation of the iPP chains parallel to the oriented $CaSt_2$ particles. X-Ray beam is perpendicular to the cross-section of the tensile bar.

Fig. 7b). The concentration gradient of the $CaSt_2$ particles affects the performance of the material. As noted in Table 3, for the case of iPP-$CaSt_2$20, a lower concentration of $CaSt_2$ is observed at different regions of the sample due to the skin effect. At higher filler loadings, the $CaSt_2$ concentration is 20wt% on average, but it may be lower in the center and higher at the edges. This can cause the divergence of the mechanical properties in Table 3. Further work is necessary to stabilize the particle size and geometry.

As suggested by the SAXS image given in Fig. 7e, the elongated $CaSt_2$ particles force the iPP chains to orient in a direction parallel with the cocontinuous $CaSt_2$ particle domains. It is possible that this iPP chain orientation leads to the formation of iPP crystals with the $CaSt_2$ sandwiched in between.

CONCLUSION

Toughening of isotactic polypropylene was investigated by using the low molecular weight additive calcium stearate. $CaSt_2$ was melt blended with iPP where the characteristic cocontinuous morphology of $CaSt_2$ additive increased the melt flow rate dramatically at the processing temperatures. Once cooled, mesomorphic $CaSt_2$ coassembled with the iPP matrix generating spherical domains in the bulk, and elongated ellipsoidal particles at the free surfaces of the specimen as a result of the skin effect. The sizes of the reinforcing domains increase with increasing weight fraction of the filler.

Although the crystallinity of iPP matrix was reduced with the incorporation of calcium stearate, a slight change in the crystal lattice structure was observed. Furthermore, contrary to expected decrease in modulus due to reduced crystallinity, the complex behavior of $CaSt_2$ filler stiffened the iPP matrix. Addition of 10% $CaSt_2$ increased the flexural modulus by ~20%. Intricate $CaSt_2$ morphology is suggested to form coassembled domains of $CaSt_2$ and iPP which increased the fracture energy of the iPP matrix by almost four-fold, producing a supertough composite at relatively low filler volume fractions (9%). These results suggest that the synergism of $CaSt_2$ additive within the iPP matrix demonstrates that $CaSt_2$ is a potential filler to tremendously increase the fracture energy and stiffness while improving processing conditions of the material significantly.

ACKNOWLEDGMENTS

The authors gratefully thank Braskem SA for financial support, materials provided and use of their facilities.

REFERENCES

1. R.J. Gaymans, "Toughening of Semi-crystalline Thermoplastics," in *Polymer Blends, Vol. 2: Performance*, D.R. Paul and C.B. Bucknall, Eds., Wiley, New York (1999).
2. Z. Bartczak, A.S. Argon, R.E. Cohen, and M. Weinberg, *Polymer*, **40**, 2347 (1999).
3. S. George, K. Ramamurthy, J.S. Anand, G. Groeninckx, K.T. Varughese, and S. Tabu, *Polymer*, **40**, 4325 (1999).
4. A.J. Lesser, T.J. McCarthy, J. Yoon, and O.S. Yordem, U.S. Patent 2008/058618 (2008).

5. J. Yoon, T.J. Mccarthy, and A.J. Lesser, *J. Appl. Polym. Sci.*, **113**, 3564 (2009).
6. S.B. Elliott, *The Alkaline-Earth and Heavy-Metal Soaps*, Reinhold Publishing Corporation, New York (1946).
7. M.C. Mehrotra and R. Bohra, *Metal Carboxylates*, Academic Press, London (1983).
8. H.S. Makowski and R.D. Lundberg, Polymer Preprints (American Chemical Society, Division of Polymer Chemistry), **19**(**2**), 304 (1978).
9. H.S. Makowski, P.K. Agarwal, R.A. Weiss, R.D. Lundberg, Polymer Preprints (American Chemical Society, Division of Polymer Chemistry), **20**(**2**), 281 (1979).
10. I. Duvdevani, R.D. Lundberg, C. Wood-Cordova, G.L. Wilkes, ACS Symposium Series (Coulombic Interact. Macromol. Syst.), Chapter 15, **302**, 184 (1986).
11. D.A. Jackson, J.T. Koberstein, and R.A. Weiss, *J. Polym. Sci. Pt. B-Polym. Phys.*, **37**, 3141 (1999).
12. R.A. Weiss, *J. Appl. Polym. Sci.*, **28**, 3321 (1983).
13. R.A. Weiss, E. Izzo, and S. Mandelbaum, *Macromolecules*, **41**, 2978 (2008).
14. K. Wakabayashi and R.A. Register, *Polymer*, **47**, 2874 (2006).
15. Riley, *J. Vinyl Technol.*, **5**, 132 (1999).
16. V. Luzzati, *Biological Membranes*, Academic Press, London (1968).
17. R.D. Vold, J.D. Grandline II, and M.J. Vold, *J. Colloid Sci.*, **3**, 339 (1948).
18. D.R. Gee and T.P. Melia, *Die Makromolekulare Chemie*, **132**, 195 (1970).
19. O.S. Yordem and A.J. Lesser, *J. Polym. Sci. Pt. B-Polym. Phys.*, **48**, 840 (2010).
20. J. Yoon, A.J. Lesser, and T.J. Mccarthy, *Macromolecules*, **42**, 8827 (2009).
21. Y.S. Thio, A.S. Argon, R.E. Cohen, and M. Weinberg, *Polymer*, **43**, 3661 (2002).
22. M. Fukushima and T. Iwanami, U.S. Patent 3,926,876 (1975).

 DOI 10.1002/pen